Measuring stiffness and residual stress of thin films with contact resonance atomic force microscopy

Chengfu Ma,[1,2] Yuhang Chen,[1*] Jianfeng Chen,[1,2] and Jiaru Chu[1]

[1] Department of Precision Machinery and Precision Instrumentation, University of Science and Technology of China, Hefei 230026, Anhui, China

[2] USTC center for Micro- and Nanoscale Research and Fabrication, University of Science and Technology of China, Hefei 230026, Anhui, China

E-mail: chenyh@ustc.edu.cn

ABSTRACT

A method based on contact resonance atomic force microscopy was proposed to determine the mechanical properties of thin films. By analyzing contact resonance frequencies of an AFM probe while the tip-sample is in contact, stiffness and residual stress of a freestanding circular SiN_x membrane were evaluated quantitatively. The obtained magnitude of residual stress was in reasonable accordance with that from wafer curvature measurement. The method was verified to have much better mechanical sensitivity than the popular AFM bending test method. And its promising application on fast, nondestructive mechanical mapping of thin-film-type structures at the nanoscale was also demonstrated.

PLEASE CITE THIS ARTICLE AS DOI: 10.7567/APEX.9.116601

With the rapid development of nanoscience and nanotechnology, thin films have been extensively applied in a wide range of fields, including microelectromechanical systems, sensors and actuators, optical devices and so on.[1-4] Among their many concerned characteristics, the mechanical properties are of fundamental importance for reliable device performances. Therefore, there is an urgent demand for developing fast, nondestructive and quantitative characterization methods. Unfortunately, due to different thermal expansion coefficients between the deposited material and the substrate, residual stress presents commonly in prepared thin films, which will greatly affect their mechanical behaviors and make the characterization more challenging.[5] To measure the mechanical properties of thin films, especially the residual stress, several techniques have been developed, such as wafer curvature measurement,[6] bugle test,[7] nanoindentation,[8] resonant based techniques,[9] and X-ray method.[10] In case of 2D material films and nanowire beams, atomic force microscopy (AFM) static point-deflection method is attracting more and more attention owing to its ultrahigh force and displacement resolutions.[11,12] However, only by utilizing a probe having a matching force constant with the stiffness of the investigated film, can satisfactory accuracy be acquired.

Acoustic-based AFM techniques, which combine contact mode AFM with ultrasonic frequency vibrations, have emerged as powerful tools for mechanical characterization of materials in the past two decades. Such techniques have already been successfully applied to study the elastic properties of advanced materials, detect subsurface defects and nanostructures, and explore interface characteristics.[13-16] Among which, by recording the contact resonance (CR) frequencies and by subsequent analyzing with proper tip-sample contact model and cantilever dynamic model, quantitative mechanical characterizations can be realized with CR-AFM techniques. However, most of such investigations focused on evaluation of the elastic modulus

or stiffness while few publications concerned the residual stress until now. In this letter, we proposed a new method to study the mechanical properties, especially the residual stress, of thin films with CR-AFM techniques. The stiffness distribution of a freestanding circular SiN_x membrane was firstly measured. Then, the residual stress was evaluated by modeling the mechanics of the pre-stressed circular membrane under a point load. The obtained residual stress value was in reasonable agreement with that from wafer curvature test. The method was verified to have much better mechanical response sensitivity than quasi-static AFM bending test method. And its capability for fast, nondestructive mechanical mapping at nanoscale was also demonstrated, which is quite appealing especially for applications on nano-films with irregular shapes, heterogeneous mechanical properties, or defects.

The schematic illustration of exploiting CR-AFM on mechanical characterization of thin films is shown in Figure 1. The following experiments were performed on a commercial AFM platform (MFP-3D Origin, Asylum Research, Santa Barbara, CA) with the ultrasonic excitation applied on the probe, that is the so-called ultrasonic-AFM (UAFM) mode.[17] By recording the CR spectra with the lock-in amplifier under a sweeping frequency excitation, CR frequencies at different positions on the membrane can be obtained, which are relevant to local stiffness and modulus. Additionally, by oscillating the probe around one of the CR frequencies while the tip is scanning on the surface, and by extracting the amplitude and phase signals, a qualitative mechanical mapping of the membrane can be realized. Furthermore, with aiding techniques such as Dual AC™ Resonance Tracking (DART),[18] CR frequency image can also be easily acquired which can be quantitatively converted into corresponding mechanical properties maps.

A thin clamped freestanding circular SiN_x membrane was fabricated to test the method, as the process described in Fig. S1 in the supplementary material. The measurements started with a

demonstration of the mechanical characterization ability based on CR-AFM. The tested membrane was determined to have a thickness of 524 ± 0.9 nm after a wafer-scale measurement with a film thickness mapping tool (SRM300, Angstrom Sun Technologies, Acton, MA), and a diameter of about 504 μm by an optical microscope. As shown in the optical view in Fig. 2(a), a ContAl-G cantilever (BudgetSensors, Innovative Solutions Bulgaria Ltd., Bulgaria) was first brought into contact with sample surface, and then CR spectroscopy and UAFM imaging were applied. Before the measurements, the inverse optical lever sensitivity was determined to be 157.6 nm/V, and the spring constant of the cantilever was 0.28 N/m by thermal calibration.[19] The first four free resonance (FR) frequencies of the cantilever were respectively 14.4 kHz, 91.6 kHz, 252.6 kHz, and 495.1 kHz. And all the experiments were conducted under a tip load of approximately 88 nN.

Then CR spectra tests were conducted on the substrate and at the membrane center area respectively. As shown in Fig. 2(b), the first three CR frequencies were around 79 kHz, 230 kHz, and 450 kHz. And it can be unambiguously seen that there was much larger frequency shift for the 3rd CR eigenmode than the 1st and 2nd modes, with the frequency at the center smaller than the one on the substrate. Actually, as compared with those on the substrate, the first three CR frequencies at the center were respectively no difference, 8 kHz smaller, and 35 kHz smaller approximately (see Fig. S2). This indicates that the 2nd and 3rd CR modes have considerable better sensitivities, where the 3rd one has the best, to the mechanical difference between the solid substrate and the freestanding membrane. Consequently, the 3rd CR mode was chosen in following experiments. Next, to demonstrate the mechanical mapping capability of CR-AFM, a UAFM scan was applied with the drive frequency set at 440 kHz around the 3rd CR frequency. Figures 2(c)-(e) show the obtained topography, amplitude and phase images in the 90 μm × 90

μm scan area around the membrane periphery. It can be found that the amplitude and phase images can unambiguously distinguish the freestanding membrane from the substrate, which is not visible from the topography.

To characterize the stiffness distribution of the membrane, CR spectra were swept at different positions along its radial axis, as illustrated in Fig. 1. Figure 3(a) shows the 3rd CR frequencies extracted from these spectra, which has a bowl-shaped distribution along the membrane's radial direction indicating that the membrane center area has the lowest stiffness, and there is a rapid increase of the stiffness while moving to the periphery.

A simplified analytical model of the cantilever in contact with the sample, as schematically shown in Fig. 3(b), was used to convert the measured CR frequencies to contact stiffness values. Both the normal and lateral contact interactions (represented by k_N and k_L respectively), the cantilever tilt of α_0 induced by the mounting angle of the cantilever holder, and the tip position (L_1, L_2) and height h were considered. The characteristic Euler-Bernoulli equation describing the transverse flexural vibration of the cantilever is,

$$EI\frac{\partial^4 y(x,t)}{\partial x^4} + \rho A\frac{\partial^2 y(x,t)}{\partial t^2} = 0, \tag{1}$$

where E is the Young's modulus, I is the area moment of inertia, ρ is the mass density and A is the sectional area. $y(x,t)$ denotes the cantilever deflection and the general solution is in form of,

$$y(x,t) = \left(a_1 e^{\lambda x} + a_2 e^{-\lambda x} + a_3 e^{i\lambda x} + a_4 e^{-i\lambda x}\right)e^{i\omega t}. \tag{2}$$

Here, ω is the angular frequency, λ is the wave number. Constant parameters a_1, a_2, a_3 and a_4 can be determined from the boundary conditions. First, the deflection and the slope are zero at the clamped end. Second, no moment and shear force present at the free end. Last, the tip-sample interactions k_N and k_L induce corresponding shear force and bending moment, and deflection

and slope should be continuous for the two cantilever sections L_1 and L_2 at the tip position. Combing the characteristic equation and the boundary conditions, the contact stiffness is computed by numerically solving the equation:[20)]

$$\frac{C}{3}\frac{k_C}{k_N} + B_1 + B_2\frac{k_L}{k_N} + 3A\frac{k_L}{k_N}\frac{k_N}{k_C} = 0, \tag{3}$$

where

$$A = \left(\frac{h}{L_1}\right)^2 (1 - \cos(\lambda_n L_1)\cosh(\lambda_n L_1))(1 + \cos(\lambda_n L_2)\cosh(\lambda_n L_2)), \tag{4}$$

$$B_1 = \sin^2\alpha_0\, B_1^* - B_2^* + \cos^2\alpha_0\, B_3^*, \tag{5}$$

$$B_2 = \cos^2\alpha_0\, B_1^* + B_2^* + \sin^2\alpha_0\, B_3^*, \tag{6}$$

$$C = 2(\lambda_n L_1)^4(1 + \cos(\lambda_n L)\cosh(\lambda_n L)), \tag{7}$$

with

$$B_1^* = \left(\frac{h}{L_1}\right)^2 (\lambda_n L_1)^3[(1 + \cos(\lambda_n L_2)\cosh(\lambda_n L_2)\,(\sin(\lambda_n L_1)\cosh(\lambda_n L_1) + \cos(\lambda_n L_1)\sinh(\lambda_n L_1)) - (1 - \cos(\lambda_n L_1)\cosh(\lambda_n L_1)\,(\sin(\lambda_n L_2)\cosh(\lambda_n L_2) + \cos(\lambda_n L_2)\sinh(\lambda_n L_2))], \tag{8}$$

$$B_2^* = \left(\frac{h}{L_1}\right)(\lambda_n L_1)^2 \sin\alpha_0\cos\alpha_0\,[(1 + \cos(\lambda_n L_2)\cosh(\lambda_n L_2))\sin(\lambda_n L_1)\sinh(\lambda_n L_1) + (1 - \cos(\lambda_n L_1)\cosh(\lambda_n L_1))\sin(\lambda_n L_2)\sinh(\lambda_n L_2)], \tag{9}$$

$$B_3^* = \lambda_n L_1[(1 + \cos(\lambda_n L_2)\cosh(\lambda_n L_2))(\sin(\lambda_n L_1))\cosh(\lambda_n L_1) - \cos(\lambda_n L_1)\sinh(\lambda_n L_1) - (1 - \cos(\lambda_n L_1)\cosh(\lambda_n L_1))(\sin(\lambda_n L_2)\cosh(\lambda_n L_2) - \cos(\lambda_n L_2)\sinh(\lambda_n L_2))]. \tag{10}$$

Here, $\lambda_n L$ is the normalized wave numbers of the n^{th} flexural resonance eigenmode, and can be related with the CR frequencies f_n^c and FR frequencies f_n^0 from the dispersion equation as follows (the superscripts c and 0 respectively denote the CR and FR modes here),

$$(\lambda_n L)^c = (\lambda_n L)^0 \sqrt{\frac{f_n^c}{f_n^0}}. \tag{11}$$

In our experiments, the cantilever length L is 450 μm and the tip has a height of 17 μm and a position L_1/L of 0.9667 as provided by the manufacturer. The cantilever tilt angle is 11°. And the contact stiffness ratio k_L/k_N is estimated to be equal to $2(1-\nu)/(2-\nu)$ on the supported substrate, which yields 0.84 for a material with a Poisson's ratio ν of 0.27.[21] By submitting the measured CR frequencies on the substrate area into Eq. (3) with k_L/k_N set to be 0.84, a mean value of 468.9 N/m was determined for k_L. And as k_L will keep constant across the entire measurement, the normal contact stiffness values on the membrane can be calculated with k_L set to be 468.9 N/m.

Figure 3(c) shows the calculated relation between the 3rd CR frequency and the normal contact stiffness, respectively normalized by the 1st FR frequency and the cantilever spring constant. When we marked the experimental CR frequencies on this curve, a good sensitivity of the 3rd mode was again demonstrated. Then contact stiffness values were calculated from the corresponding experimental CR frequencies and the results were shown in Fig. 3(d). The obtained contact stiffness along the membrane's radial direction also has a bowl-shaped distribution, with the magnitudes range from about 558 N/m on the substrate to about 196 N/m at the membrane center.

Then, the stiffness of the membrane was calculated by considering the model of a vibrating cantilever contacting a membrane as shown in Fig. 4(a). Overall deflection of the membrane

(structure) and local deformation of the material (material) exist during the measurement, both of which are assumed to be elastic under such small loading forces. Therefore, the contact stiffness k_N can be regarded as series of membrane deflection stiffness k_S and material deformation stiffness k_M, that is $1/k_N=1/k_S+1/k_M$. Since there is no membrane deflection on the substrate area, that is $k_S \rightarrow \infty$, we get $(1/k_N=1/k_M)_{substrate}$. And this leads to $(1/k_S)_{membrane}=(1/k_N)_{membrane}-(1/k_N)_{substrate}$. Thus, by assigning $(k_N)_{membrane}$ with the mean contact stiffness obtained on the substrate area, the membrane stiffness $(k_S)_{membrane}$ can be evaluated from previously calculated contact stiffness values. Figure 4(b) displays the derived membrane stiffness at various positions along the radial direction, indicating a minimum stiffness of 302.5 N/m at the center and a sharp increase around the periphery. Such large a stiffness of the membrane strongly implies the existence of tensile residual stress.

To determine the residual stress of the membrane, modeling the mechanics of a pre-stressed circular membrane is necessary. The deflection at the center of a circular membrane under a vertical point load P at the center and a radial tensile force per unit length N at the edge can be expressed as,[22)]

$$w = \frac{PR^2}{16\pi D} g(k), \tag{12}$$

where,

$$g(k) = \frac{8}{k^2}\left[\frac{\left\{K_1(k)-\frac{1}{k}\right\}}{I_1(k)} \cdot \{I_0(k)-1\} + K_0(k) + \ln\left(\frac{k}{2}\right) + \gamma\right], \tag{13}$$

and $D = Et^3/12(1-v^2)$ is the flexural rigidity of the membrane, with E the Young's modulus, t the thickness, v the Poisson's ratio; $k^2 = NR^2/D$ is a defined coefficient, with R the membrane radius; I_0 and I_1 are respectively the modified Bessel function of the first kind of order 0 and 1, and K_0 and K_1 respectively the modified Bessel function of the second kind of order 0 and 1; γ is

Euler's constant. Thus the stiffness of a circular membrane at the center, that is the load-deflection slope P/w, is determined by the radius R, thickness t, Young's modulus E and the residual stress σ ($\sigma = N/t$). Figure 4(c) shows the calculated center stiffness values of membranes with various residual stresses and Young's moduli. In calculation, the radius and thickness were fixed at 252 μm and 524 nm respectively. It can be found that the membrane stiffness increases dramatically with the increase of the residual stress. However, the stiffness is much less sensitive to Young's modulus. This makes it possible to determine the residual stress accurately enough by taking a reasonable assumption of the Young's modulus. Here, Young's modulus of the tested SiN_x membrane was set within 150-250 GPa, which was the most frequently reported values according to literatures for thin films with the same fabrication process.[23,24] Then, by matching the calculated load-deflection slopes with the obtained membrane stiffness at the center, 302.5 N/m, the residual stress was finally determined to be in a range of 366-393 MPa.

In addition, a thoroughly uncertainty analysis of our method was performed. All the experimental and model parameters were considered in the analysis by taking random deviations with relatively large enough ranges for them, as listed in Table I. Then one thousand times calculations of the obtained residual stress were applied, and the results are shown in Fig. 4(d). A mean value of 374 MPa and a standard deviation of 39 MPa of the residual stress were determined which indicate a quite good stability of the method.

The experimental results indicate that the developed CR-AFM spectroscopy based tests can be used to characterize the stiffness and residual stress of thin films simultaneously. The method was first compared with the quasi-static AFM based bending test. Force-displacement tests were performed in-situ during the CR spectroscopy experiments. Unlike the 2nd and 3rd mode CR

spectra, the results show that the AFM bending tests can even hardly reveal the existence of the freestanding membrane, as demonstrated in Fig. S2. That is to say, the CR method has much better mechanical sensitivity. Then, the obtained residual stress was compared with the one determined by the widely-used wafer curvature test on another SiN_x membrane fabricated with the same processing conditions but with a little difference in the film thickness. A Stylus Profiler system (Dektak XT, Bruker Corporation, Billerica, MA) was used to measure the residual stress, which gave an averaged stress of 372 MPa with a standard deviation of about 59 MPa within an 80 mm long profile (see Fig. S3). This ascertain that the acquired residual stress of 366-393 MPa is in reasonable agreement with that from the conventional wafer curvature test.

In summary, a method based on CR-AFM techniques was proposed to study the stiffness distribution and residual stress of a freestanding circular SiN_x membrane. The method was demonstrated to have much better mechanical sensitivity than the popular quasi-static AFM bending test. And the obtained residual stress value was verified to be in good accordance with that from wafer curvature test. In addition, the ability of CR-AFM for fast, nondestructive mechanical mapping of thin films at the nanoscale was also demonstrated. This paves a way for simultaneous measurement of modulus, stiffness and residual stress of thin films at the nanoscale. And it has potential applications in film-based micro-and-nano devices, including those of 2D-materials.

ACKNOWLEDGEMENTS

This work was financially supported by the research grant (Nos. 51275503 and 51675504) from the National Natural Science Foundation of China. The authors acknowledge the technical support from USTC center for Micro- and Nanoscale Research and Fabrication.

REFERENCES

1) Y. Fu, H. Du, W. Huang, S. Zhang, and M. Hu, Sensor. Actuat. A-Phys. **112**, 395 (2004).
2) K. Lee, R. Gatensby, N. McEvoy, T. Hallam, and G. S. Duesberg, Adv. Mater., **25**, 6699 (2013).
3) C. C. Striemer, T. R. Gaborski, J. L. McGrath, and P. M. Fauchet, Nature, **445**, 749 (2007).
4) C. Reinhardt, T. Müller, A. Bourassa, and J. C. Sankey, Phys. Rev. X, **6**, 021001 (2016).
5) C. C. Lee, G. Z. Cao, and I. Y. Shen, Sensor. Actuat. A-Phys., **159**, 88 (2010).
6) C. A. Klein, J. Appl. Phys., **88**, 5487 (2000).
7) E. I. Bromley, J. N. Randall, D. C. Flanders, and R. W. Mountain, J. Vac. Sci. Technol. B, **1**, 1364 (1983).
8) G. M. Pharr, and W. C. Oliver, MRS Bull., **17**, 28 (1992).
9) S. Ma, S. Wang, F. Iacopi, and H. Huang, Appl. Phys. Lett. **103**, 031603 (2013).
10) U. Welzel, J. Ligot, P. Lamparter, A. C. Vermeulen, and E. J. Mittemeijer, J. Appl. Cryst. **38**, 1 (2005).
11) Y. Calahorra, O. Shtempluck, V. Kotchetkov, and Y. E. Yaish, Nano Lett., **15**, 2945(2015).
12) Y. Gao, Y. J. Sun, and T. Y. Zhang, Appl. Phys. Lett., **108**, 123104 (2016).
13) T. Tsuji, and K. Yamanaka, Nanotechnology, **12**, 301 (2001).
14) G. S. Shekhawat, and V. P. Dravid, Science, **310**, 89 (2005).
15) D. C. Hurley, M. Kopycinska-Müller, E. D. Langlois, A. B. Kos, and N. Barbosa, Appl. Phys. Lett., **89**, 1911 (2006).
16) Z. Parlak, Q. Tu, and S. Zauscher, Nanotechnology, **25**, 445703 (2014).
17) C. Ma, Y. Chen, T. Wang, and J. Chu, Scanning **37**, 284 (2015).

18) A. Gannepalli, D. G. Yablon, A. H. Tsou, and R. Proksch, Nanotechnology **22**, 355705 (2011).

19) J. E. Sader, J. W. Chon, and P. Mulvaney, Rev. Sci. Instrum., **70**, 3967(1999).

20) D. C. Hurley, and J. A. Turner, J. Appl. Phys. **102**, 033509 (2007).

21) P. E. Mazeran, andJ. L. Loubet, Tribol. Lett. **7**, 199 (1999).

22) S. Hong, T. P. Weihs, J. C. Bravman, and W. D. Nix, J. Electron. Mater. **19**, 903 (1990).

23) H. Huang, K. J. Winchester, A. Suvorova, B. R. Lawn, Y. Liu, X. Z. Hu, J. M. Dell, and L.Faraone, Mater. Sci. Eng. A-Struct., **435**, 453 (2006).

24) J. A. Taylor, J. Vac. Sci. Technol. A, **9**, 2464 (1991).

FIGURE CAPTIONS

FIG. 1. Schematic illustration of exploiting CR-AFM on mechanical characterization of a freestanding circular thin film.

FIG. 2. (a) Optical view of the cantilever and membrane sample with CR spectroscopy test positions and the UAFM scan area illustrated. (b) Frequency spectra in air, in contact with the substrate and at the membrane center. (c)-(e) UAFM topography, amplitude, and phase images.

FIG. 3. (a) Extracted 3rd CR frequencies under various positions along the radial direction. (b) A simplified analytical model of the cantilever in contact with the sample. (c) Relationships between the normalized 3rd CR frequency and the normalized contact stiffness. The experimental obtained CR frequencies were marked on the curve. (d) Calculated contact stiffness values.

FIG. 4. (a) Schematic illustration of the vibrated cantilever contacting with the membrane. (b) Obtained deflection stiffness values at various positions along the radial direction of the membrane. (c) Calculated stiffness values at the membrane center with various residual stresses and Young's moduli. (4) Values of the residual stress of one thousand times calculations in uncertainty analysis.

TABLES

Table I. Parameters with their mean values and deviations considered in the uncertainty analysis.

Parameter	Symbol	Unit	Mean value	Deviation
Cantilever length	L	µm	450	±10
Tip position	L_1/L	—	0.9667	±0.0111
Tip height	h	µm	17	±2
Cantilever tilt	α_0	°	11	±2
Cantilever stiffness	k_C	N/m	0.28	±0.014
1st FR frequency	f_1^0	kHz	14.4	±0.5
CR frequencies	f_n^c	kHz	—	±2
Membrane radius	R	µm	252	±10
Membrane thickness	t	nm	524	±5
Young's modulus	E	GPa	200	±50
Poisson's ratio	ν	—	0.27	±0.02

FIGURES

FIG. 1

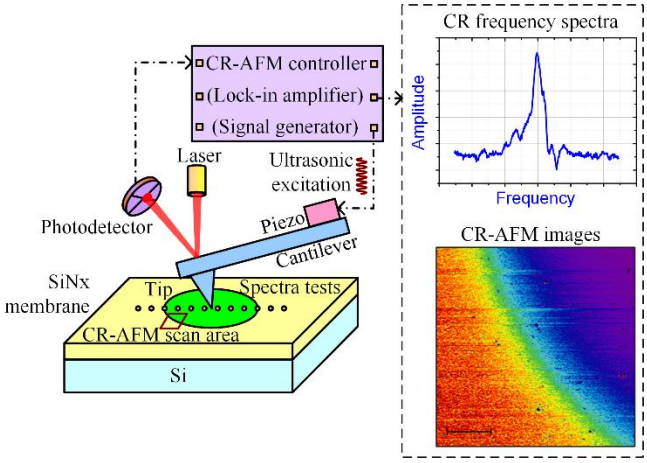

FIG. 2

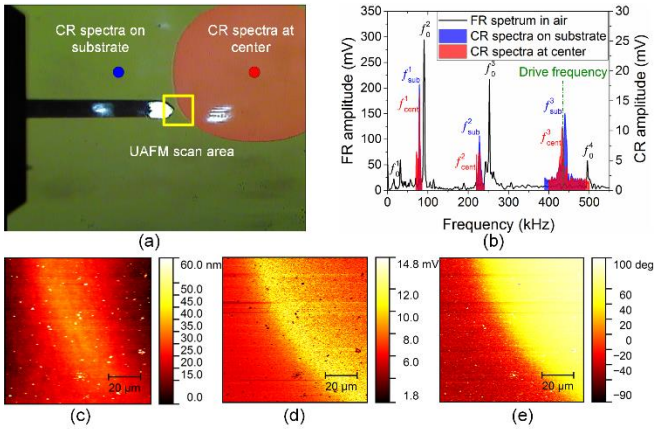
CR spectra on substrate
CR spectra at center
UAFM scan area
(a)
FR spetrum in air
CR spectra on substrate
CR spectra at center
Drive frequency
FR amplitude (mV)
CR amplitude (mV)
Frequency (kHz)
(b)
60.0 nm
50.0
45.0
40.0
35.0
30.0
25.0
20.0
15.0
0.0
20 μm
(c)
14.8 mV
12.0
10.0
8.0
6.0
1.8
20 μm
(d)
100 deg
60
40
20
0
−20
−40
−90
20 μm
(e)

FIG. 3

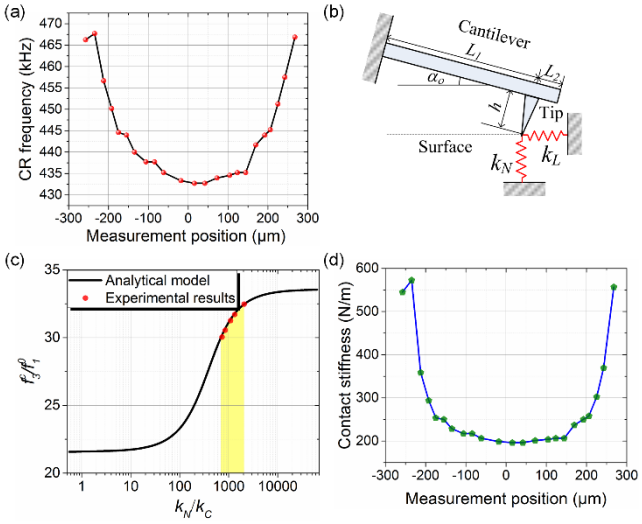
(a)
CR frequency (kHz)
Measurement position (μm)
(b)
Cantilever
L_1
L_2
α_o
h
Tip
Surface
k_N
k_L
(c)
Analytical model
Experimental results
f_3^c/f_1^0
k_N/k_C
(d)
Contact stiffness (N/m)
Measurement position (μm)

FIG. 4

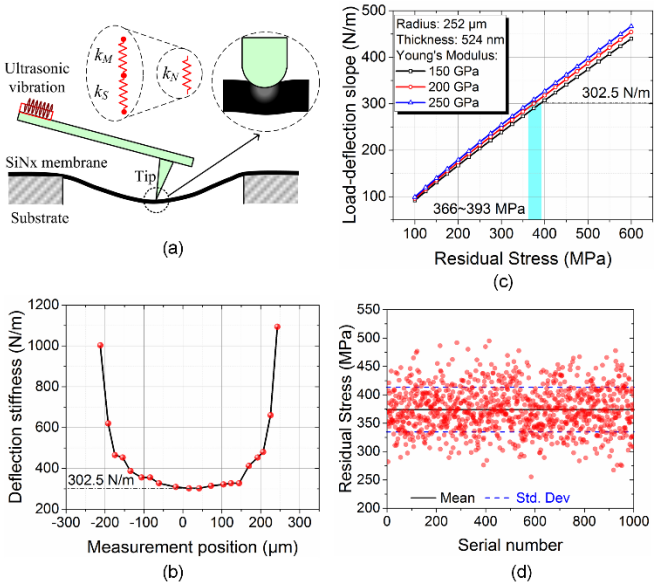
Ultrasonic vibration
k_M
k_S
k_N
SiNx membrane
Tip
Substrate
(a)
Radius: 252 μm
Thickness: 524 nm
Young's Modulus:
150 GPa
200 GPa
250 GPa
302.5 N/m
366~393 MPa
Load-deflection slope (N/m)
Residual Stress (MPa)
(c)
Deflection stiffness (N/m)
302.5 N/m
Measurement position (μm)
(b)
Residual Stress (MPa)
Mean
Std. Dev
Serial number
(d)